MINERALOGICAL, PETROLOGICAL AND PHYSICAL PROPERTIES OF RYUGU SAMPLES USING X-RAY NANOTOMOGRAPHY.

A. Tsuchiyama[1,2], M. Matsumoto[3], J. Matsuno[1], T. Nakamura[3], T. Noguchi[4,5], K. Uesugi[6], A. Takeuchi[6], M. Yasutake[6], A. Miyake[4], S. Okumura[4], Y. Fujioka[3], M. Sun[2], A. Takigawa[7], T. Matsumoto[4], S. Enju[8], I. Mitsukawa[4], Y. Enokido[3], T. Kawamoto[9], T. Michikami[10], T. Morita[3], M. Kikuiri[3], K. Amano[3], E. Kagawa[3], N. Nakano[4], S. Rubino[11], T. Nakano[12] H. Yurimoto[13], R. Okazaki[5], H. Yabuta[14], H. Naraoka[5], K. Sakamoto[15], S. Tachibana[7,15], S. Watanabe[16], Y. Tsuda[15] and the Hayabusa2-initial-analysis Stone and Sand teams, [1]Ritsumeikan University, Japan, [2]CAS, Guangzhou Institute of Geochemistry, China, [3]Tohoku University, Japan, [4]Kyoto University, Japan, [5]Kyushu University, Japan, [6]SPring8/JASRI, Japan, [7]University of Tokyo, Japan, [8]Ehime University, Japan, [9]Shizuoka University, Japan, [10]Kinki University, Japan, [11]IAS, Université Paris-Saclay, CNRS, France, [12]GSA/AIST, Japan, [13]Hokkaido University, Japan, [14]Hiroshima University, Japan, [15]ISAS/JAXA, Japan, [16]Nagoya University, Japan. (atsuchi@fc.ritsumei.ac.jp)

Introduction: Samples collected from the asteroid 162173 Ryugu by the Hayabusa2 spacecraft were successfully recovered on the Earth in December 2020. We have performed nondestructive analysis of these samples in 3D using SR-based X-ray nanotomography (XnCT) as parts of the Hayabusa2 initial analysis "Stone" team [1] and "Sand" team [2].

Methods: We examined 39 and 36 samples (10 ~ 180 µm in apparent size) from Chambers A and C, respectively, were picked up from sample canisters without crashing ([1] and some of [2]) or removed from large grains [2]. Some particles have been examined by FTIR [1,3] prior to X-nCT and also by SR-based XRF [1]. Inclusions in FeS and breunnerite grains were examined by TOF-SIMS [1,4] and microRaman, respectively. After the X-nCT measurements, ultra-thin sections of regions of interest were extracted from some samples based on the X-nCT results by FIB and observed by (S)TEM/EDS [5].

Most of the samples were imaged by two different methods (dual-energy tomography (DET) [6] and scanning-imaging X-ray microscopy (SIXM) [7]) at BL47XU of SPring-8 [8]. In DET, absorption contrast images of linear attenuation coefficient (LAC) were obtained at 7 and 7.35 keV, which correspond closely to compositional (Z) and Fe contrasts, respectively. In SIXM, we obtained X-ray differential phase contrast images of refractive index decrement (RID) at 8 keV. RID is the difference between the X-ray refractive index (RI) and unity (RID = 1 - RI) and closely proportional to the density. The voxel sizes of the LAC and RID images are ~50 and ~110 nm, respectively.

Image analysis: Image analysis was performed by combining ImageJ and codes made with C and Python. After registration among the three types of images, RGB-CT images were made by merging LAC 7 keV, LAC 7.35 keV, and RID images as blue, red, and green, respectively (Fig. 1). Different phases are shown by different colors in these images. Minerals and IOM can be discriminated by comparing the LAC and RID values of the objects in CT images to those of known minerals. The average density and Mg# (=Mg/[Mg+Fe]) of matrix were estimated form the LAC and RID values of matrix by assuming the matrix is simply composed of serpentine solid solution, organics, and void.

The solid portions of the particles were extracted from LAC 7.35 keV images using Chan-Base segmentation. The volume, surface area, 3-axial lengths ($A{\geq}B{\geq}C$), and fractal dimension were obtained. Porosity including pores and cracks open to the outside, p, was estimated by a wrapping method [9]. The grain density, ρ_g, was estimated from the average RID value of the solid portion and the bulk density, ρ_b, by $\rho_g{\times}(1-p)$.

Results: *Mineralogy and 3D textures.* A typical RGB-CT image is shown in Fig.1. Samples are mainly composed of Mg-rich phyllosilicates (serpentine and saponite) in matrix. On the scale of ~100 µm or smaller, the matrix is heterogeneous. Homogeneous small objects which might be pseudomorphs of olivine and/or pyroxene are present and some of them are covered with FeS crystals. Spherical objects with coarse-grained phyllosilicate mantle are also seen. The average matrix density estimated here may be affected by the presence of nanopores below the spatial resolution [5], and Mg# are different grain by grain (1.2~2.1 g/cm^3 and 0.75~0.92, respectively, N=55).
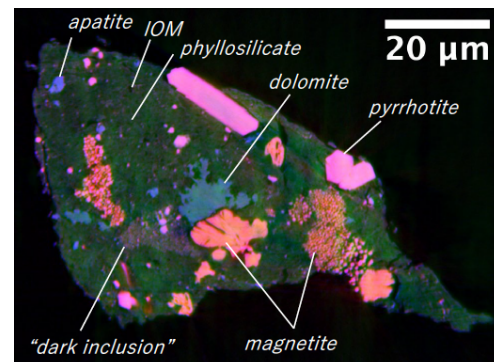

Figure 1. RGB-CT images of C0103-FC007. R: LAC at 7 keV = 0-950 cm^{-1}, G: RID = 0-20${\times}$10^{-6}, B: LAC at 7.35 keV = 0-450 cm^{-1}.

Pyrrhotite is commonly present as a hexagonal plate as well as minor pentlandite. Fe(-Ni)S nanograins are also present in limited areas of matrix. Magnetite is also a common phase and has a variety of morphology; spherulites and their aggregates, framboids composed of not only sub-micron grains but also larger grains (>1 μm), plaquettes, large euhedral equant grains and elongated grains. We found several whiskers of probably magnetite (one of them was confirmed by TEM). Dolomite is usually present mostly as aggregates of euhedral to subhedral grains and sometimes as separate rhombohedral grains. Aggregates of sub-micron dolomite are also present in the matrix. Breunnerite is present as rhombohedral grains. $CaCO_3$ (probably calcite) is rarely present. Apatite is usually present mostly as aggregates of subhedral or anhedral grains. Na and Mg-bearing phosphate grain was also present. Small grains of forsterite or enstatite are rarely observed.

IOMs were identified commonly as small objects (sub-micron to a few μm). The mode of IOM ranges from 0.1 to 2.9 vol.% (1.2 vol.% on average, N=46). Object composed of Fe-rich and mostly anhydrous silicates, fine grains of FeS and/or magnetite named "dark inclusion" (~10 μm) and porous objects (~5 μm) like the ultra-porous lithology in Acfer 094 [8] were also recognized.

The precipitation order of major minerals was estimated based on their relative enclosing relations in 3D as follows; magnetite → pyrrhotite (hexagonal plate) → apatite → dolomite/breunnerite. Among magnetite, the order is likely spherulitic → plaquette/ framboidal (from fine to coarse) → equant/elongated.

Inclusions. FeS, dolomite, breunnerite and apatite grains have inclusions occupied by low density materials in CT images. Most of them seem to be IOM. CO_2-bearing fluid inclusion was discovered in pyrrhotite grain (C0002-FC012) by TOF-SIMS [1,4]. IOM inclusions were confirmed in breunnerite grains (A0067-FC003 and FC004) by microRaman.

Surface properties. Particles are irregular in shape and generally have concave portions. Some surfaces are jagged while some are smooth. Rounded edges by abrasion as observed on Itokawa particles [9] were not clearly observed. Melt splashes observed by SEM and TEM [2] were also recognized on some surfaces.

Physical properties. The 3D shape distribution of particles picked up from sample canisters without crashing (B/A=0.68 and C/A =0.41 on average) indicates that they are more oblate than the Itokawa particles (B/A=0.72 and C/A =0.44) and fragments of impact experiments [9], indicating that they are not simply impact fragments. Particles from Chamber C (B/A=0.70

and C/A =0.36, N=11) are more oblate than those from Chamber A (B/A=0.68 and C/A =0.44, N=21), although this difference may be within the statistical error.

Cracks less than a few μm in width are commonly present in all particles. Some cracks develop along the boundaries of some objects and mineral grains, implying cracks by shrinkage during dehydration. Some cracks are subparallel to flattened particle surfaces probably by impact.

The porosity ranges from 1 to 18% (7.6% on average, N=46). This is smaller than that of CI chondrite Orgueil (35% [10]) probably because of the difference in spatial resolution (~100 nm in this study and ~1 nm in [10]). ρ_g and ρ_b range from 1.4 to 2.2 g/cm^3 and from 1.3 to 2.1 g/cm^3 (1.8 and 1.6 g/cm^3 on average, N=46), respectively. Averaged ρ_g is smaller than that of Orgueil (2.46 g/cm^3 [10]) while ρ_b is similar (1.57 g/cm^3 [10]).

Discussion: The examined samples resemble CI in mineralogy and texture except for the probable absence of sulfates, which may be terrestrial weathering products. The porosity and density are also consistent with those of CI. Slight difference from CI may indicate that Ryugu samples correspond to slightly less-aqueously altered material. Any feature of dehydration suggested by the on-site IR spectrum [11] was not recognized. Highly porous samples as expected from the low thermal inertia [12] were not observed.

Even though large particles (> a few mm) examined by SEM/EDX and X-ray microtomography show that Ryugu samples have different lithologies on the scale larger than the present particle size [1], we obtained almost representative features of the Ryugu samples in this work because of the large number of the particles were examined in 3D. The variations of the average density and Mg# of matrix correspond to different lithologies observed in large samples. Any significant difference among samples from Chamber A and C was not recognized except for the 3D shape distribution.

References: [1] Nakamura T. et al. (2022) *Science*, submitted. [2] Noguchi T. et al. (2022) *Science*, submitted. [3] Dionett Z. et al. (2022) *LPS LIII*. [4] Zolensky M. et al. (2022) *LPS LIII*. [5] Matsumoto M. et al. (2022) *LPS LIII*. [6] Tsuchiyama A. et al. (2013) *Geochim. Cosmochim. Acta*, 116, 5. [7] Takeuchi A. et al. (2014) *J. Synchrotron Radiat.*, 20, 793. [8] Matsumoto M. et al. (2019) *Science Advances*, 5, eaax5078. [9] Tsuchiyama A. et al. (2011) *Science*, 33, 1125. [10] Flynn G. J. et al. (2018) *Chemie der Erde*, 78, 269. [11] Kitazato K. et al. (2019) *Science*, 268, 272. [12] Okada T. et al. (2020) *Nature*, 579, 518.